Hindawi
Advances in Civil Engineering
Volume 2020, Article ID 9324935, 8 pages
https://doi.org/10.1155/2020/9324935

Research Article

Analysis of Cyclic Response of Bucket Foundations Based on Simplified Kinematic Hardening Model

Qing-lai Fan, Guo-feng Xiao, and Xiao-di Chen

School of Civil Engineering, Ludong University, Yantai 264025, China

Correspondence should be addressed to Qing-lai Fan; fanqinglai@foxmail.com

Received 3 February 2020; Accepted 4 June 2020; Published 22 June 2020

Academic Editor: Qiang Tang

The response of bucket foundations for offshore wind turbines subjected to cyclic loading in saturated clay is explored through three-dimensional finite element numerical analyses. In the analyses, nonlinear cyclic hysteretic behavior of clay under undrained condition is modeled through a simple kinematic hardening constitutive model embedded in ABAQUS. The finite element model is validated against published in situ tests of bucket foundations under quasistatic cyclic loading in Bothkennar clay. The computed results agreed generally with those from in situ tests. The behavior of bucket foundations with different aspect ratios under displacement-controlled cyclic loading mode is investigated. Then, the evolution of foundation displacement with increasing number of cycles is studied subjected to wind and wave combined loading. The results show that, for the cycles of low-amplitude rotation, dimensionless moment-rotation curve is approximately elastic; however, the curve engenders obvious hysteresis loop, whose shape is influenced by soil-sidewall interface condition, during high-amplitude cycles. Under thousands of loading cycles, for bucket foundations of low aspect ratio, the oscillatory displacement component is smaller; however, the residual component will accumulate gradually until the serviceability rotation is exceeded. For foundations of high aspect ratio, the oscillatory component is relatively larger, but the accumulation rate of residual displacement decreases gradually.

1. Introduction

With the gradual consumption of nonrenewable resources and the increasing power shortage, international efforts are being made to develop offshore wind power. As a novel type of marine foundation, bucket foundation has gradually been widely utilized in construction of offshore wind turbines [1]. The forces exerted on the bucket foundation for offshore wind turbines vary greatly from those of offshore platform. The vertical load from the upper tower and turbine blade is relatively small, while the horizontal load and moment component is larger. Moreover, the bucket foundation for offshore wind turbines is subjected to repeated loads for a large number of cycles during its service life [2]. The soil around the foundation may produce plastic strain accumulation and excessive displacement, thus deteriorating the normal operation of turbines. It is noted that long-term cyclic response is typically important design situation in the wind industry, whereas bearing capacity is dominating the design in the oil and gas industry.

The stability of bucket foundation for offshore wind turbines under combined loading was studied by Fan et al. and Liu et al., and the characteristics of failure envelope of bucket foundations under different load components were analyzed [3, 4]. However, these works are limited to static loading and do not take into account the mechanical behavior of the foundation under cyclic loading. Kourkoulis et al. explored the cyclic response of bucket foundation in clay, but more attention is paid to seismic response and the number of cycles is not more than 10 times [5]. The behavior of bucket foundation under cyclic moment loading and inclined loading was studied, respectively, through full scale in situ test and model test in the pressure chamber [6, 7]. The relationship between stiffness and load level of the coupled system of bucket foundation and soil is obtained from these tests [6, 7]. Zhu et al. carried out high-cycle loading of bucket foundation in sandy soil and obtained the relationship between horizontal displacement as well as rotation angle of foundation and the number of cycles [8]. The long-term

dynamic loading tests of bucket foundation in sand were carried out by Bhattacharya et al. to analyze the dynamic characteristics of soil-foundation coupling system in frequency domain [9]. To study the mechanical response of bucket foundation for offshore wind turbines under cyclic loading in clay, in the paper, the kinematic hardening model is used to simulate the stress-strain relationship of saturated clay under undrained conditions. The displacement development law of bucket foundation for 3.5 MW offshore wind turbines under combined wind and wave loads is discussed preliminarily.

2. A Brief Introduction of Constitutive Models

The stress-strain relationship of saturated clay under cyclic loading is very complex. The advanced elastoplastic constitutive model based on effective stress is perfect in theoretic aspect, but it has many constitutive parameters to be measured. In the undrained analysis, Biot's consolidation equation or the constrained condition of volume change of soil body should be combined with application of such type of constitutive model. To simplify the analysis of interaction between soil and structure, saturated clay under undrained condition can be regarded as a single-phase medium, and the total stress constitutive model is adopted. Among them, Lemaitre and Chaboche proposed a simple kinematic hardening model, which has been widely used recently [10–12].

The linear elastic stress-strain relationship is adopted in the elastic part of the model, and only two parameters of elastic modulus E and Poisson's ratio ν are required. Under the undrained condition, Poisson's ratio is selected as $\nu = 0.49$.

The yield function of the model is

$$F = f\left(\sigma_{ij} - \alpha_{ij}\right) - H = 0, \tag{1}$$

where σ_{ij} is stress tensor, α_{ij} is back stress tensor, and it is also the kinematic hardening parameter of the model, which controls the movement of the yield surface in the stress space. H is the isotropic hardening parameter of the model, which denotes the size of the yield surface. Under undrained conditions, the yield of saturated clay is only related to deviatoric stress, but not to hydrostatic pressure. Therefore $f(\sigma_{ij} - \alpha_{ij})$ may be expressed as follows:

$$f\left(\sigma_{ij} - \alpha_{ij}\right) = \sqrt{\frac{3}{2}\left(s_{ij} - \alpha_{ij}^{\mathrm{dev}}\right) : \left(s_{ij} - \alpha_{ij}^{\mathrm{dev}}\right)}, \tag{2}$$

where s_{ij} is tensor of deviatoric stress and $\alpha_{ij}^{\mathrm{dev}}$ is the deviatoric component of back stress.

The plastic strain increment is determined by the associated flow rule, as shown in

$$\mathrm{d}\varepsilon_{ij}^{\mathrm{p}} = \mathrm{d}\bar{\varepsilon}^{\mathrm{p}} \frac{\partial f\left(\sigma_{ij} - \alpha_{ij}\right)}{\partial \sigma_{ij}}, \tag{3}$$

where $\mathrm{d}\varepsilon_{ij}^{\mathrm{p}}$ is the increment of plastic strain tensor and $\mathrm{d}\bar{\varepsilon}^{\mathrm{p}}$ is the equivalent plastic strain increment and can be expressed as $\mathrm{d}\bar{\varepsilon}^{\mathrm{p}} = \sqrt{(2/3)\mathrm{d}\varepsilon_{ij}^{\mathrm{p}}\mathrm{d}\varepsilon_{ij}^{\mathrm{p}}}$.

The yield stress in the model is controlled by the isotropic hardening law and the kinematic hardening law. The isotropic hardening component changes with the accumulation of equivalent plastic strain during loading, as shown in

$$H = \sigma_0 + Q\left(1 - e^{-b\bar{\varepsilon}^{\mathrm{p}}}\right), \tag{4}$$

where σ_0 is size of the initial yield surface when the plastic strain just occurs and Q and b are model parameters. The possible maximum variation of yield surface size is defined by the parameter Q. The size of the yield surface can enlarge when Q is a positive value, whereas negative value can be used to indicate strain softening of clay [12]. The rate of change of yield surface size with equivalent plastic strain is controlled by the parameter b.

The expression of the kinematic hardening component in the stress space is

$$\dot{\alpha}_{ij} = \frac{C}{H}\dot{\bar{\varepsilon}}^{\mathrm{p}}\left(\sigma_{ij} - \alpha_{ij}\right) - \eta\alpha_{ij}\dot{\bar{\varepsilon}}^{\mathrm{p}}, \tag{5}$$

where C is initial kinematic hardening modulus which can be taken as elastic modulus of soil E and η controls the rate of back stress that recovers with the accumulation of equivalent plastic strain. The term of $\eta\alpha_{ij}\dot{\bar{\varepsilon}}^{\mathrm{p}}$ in equation (5) makes the kinematic hardening law of this model nonlinear, to better simulate the behavior of soil under cyclic loading. For saturated clay under undrained conditions, its value can be determined by the following formula:

$$\eta = \frac{C}{\sigma_{\mathrm{y}} - \sigma_0}, \tag{6}$$

where σ_{y} is maximum yield stress of clay and it can be determined as $\sigma_{\mathrm{y}} = \sqrt{3}s_{\mathrm{u}}$ and s_{u} is undrained shear strength of clay, since the Mises strength failure criterion is adopted in this model. The size of initial yield surface, σ_0, can be selected as $\sigma_0 = \lambda\sigma_{\mathrm{y}} = \lambda\sqrt{3}s_{\mathrm{u}}$ following the recommendation of Anastasopoulos et al. [11]. The parameter λ can be determined by fitting the relation curve between dynamic shear modulus G and shear strain γ, which is obtained through dynamic triaxial test or cyclic direct shear test. The range of value of the parameter λ is usually between 0.1~0.3. Therefore the following equation can be used to calculate the value of η:

$$\eta = \frac{C}{\sigma_{\mathrm{y}} - \sigma_0} = \frac{E}{(1-\lambda)\sqrt{3}s_{\mathrm{u}}}. \tag{7}$$

3. Verification of In Situ Test

To verify the applicability of the kinematic hardening model used in this paper, the in situ cyclic loading test of bucket foundation carried out by Houlsby et al. [6] is numerically simulated. In this test, the bucket foundation diameter is D = 3 m and embedment depth is L = 1.5 m. The approximate mass of the bucket (including appurtenances) is 2000 kg, and the vertical load on the bucket throughout the test is augmented by a 2400 kg concrete block. The quasistatic cyclic horizontal loads are applied at the top of the A-frame by

means of a hydraulic jack placed 4.23 m above the lid of the caisson.

The effective unit weight of soil at Bothkennar is $\gamma' = 6.8\,\text{kN/m}^3$. The best estimate of the undrained shear strength is $s_u = 11.4 + 1.9z$, where s_u is in kPa and z is the depth in meters below the base of the test site. Following the recommendation of Houlsby et al. [6], the elastic modulus of soil is $E = 525s_u$. In the absence of other soil investigation results, during the numerical simulation, the parameter is selected as $\lambda = 0.1$, $Q = 0$, and $b = 1$. Then, according to equation (7), the kinematic parameter can be obtained as $\eta = 336.8$.

In the finite element model, the friction contact pair algorithm in ABAQUS package [13, 14] is utilized to simulate contact response at the soil-bucket interface. When the normal tensile stress develops at the soil-bucket interface, separation between soil and pile occurs. When the normal stress is compressive, the Coulomb friction law is used to describe the tangential friction stress as follows:

$$\tau_f = \mu\sigma_n, \tag{8}$$

where τf is the limiting friction stress on the interface, σn is the normal contact pressure, and μ is the coefficient of friction. In the paper, a value of $\mu = 0.7$ is selected. Considering the effect of construction disturbance, the soil strength at the interface of the inner and outer sides of bucket foundation is taken as αs_u, and α is reduction coefficient. Using inverse analysis for the penetration resistance of the bucket foundation in the test site, Houlsby et al. suggested that the reduction factor is taken as $\alpha = 0.5$ [6].

The comparison between the calculation results and the test results is shown in Figure 1. In this figure, M and θ are separately the bending moment and rotation angle at the center of the top of the foundation. Through comparison, it can be seen that the numerical results are generally in good agreement with that of the in situ loading test, although the kinematic hardening constitutive model used in this paper is relatively simple. The numerical results reasonably predict the hysteretic response and rotational stiffness reduction of the M-θ relationship curve. It is shown that the kinematic hardening model proposed by Lemaitre and Chaboche [10] is applicable in simulating the interaction between soil and foundation subjected to cyclic loading.

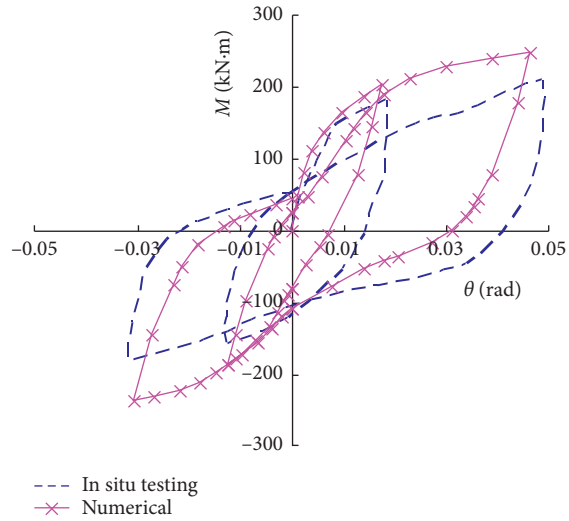

Figure 1: Relation of moment and rotation of bucket foundation in in situ tests at Bothkennar.

4. Finite Element Model

For the typical 3.5 MW offshore wind turbines, the mass of tower and wind turbine is individually $m_t = 200t$ and $m_{nr} = 220t$, and the height of the rotor center from the caisson lid is $h = 80$ m. The soil is saturated hard clay, and its effective unit weight is $\gamma' = 8\,\text{kN/m}^3$. For uniform soil, the undrained shear strength is $s_u = 60$ kPa, whereas for heterogeneous soil, the undrained shear strength increases linearly with depth z, $s_u = s_{um} + kz$, where s_{um} is the undrained strength at the seabed level, and k is linearly increasing gradient. In this paper, it is assumed that $s_{um} = 30$ kPa; $k = 2.5$ kPa/m. In the kinematic model, the parameter inputted is listed as follows: $E = 600s_u$, $\nu = 0.49$, $Q = 0$, $b = 1$, $\lambda = 0.1$, and $\eta = 384.9$. It can be seen that the soil parameter η does not change with the depth below seabed level and is a constant for both soil profiles.

The bucket foundation with diameter $D = 20$ m and wall thickness $t = 0.025$ m is considered. The developed finite element model is displayed in Figure 2 taking advantage of problem geometry symmetry. In order to reduce the boundary effect of finite element model, the diameter and thickness of soil domain are taken as $6D$ and $3D$. Soil is modeled with eight-noded hexahedral continuum elements, concentrated near the foundation.

To illustrate the influence of soil properties on the cyclic response of bucket foundation, the deformation of bucket and upper tower is not considered in the model. The bucket foundation is simulated by rigid body shell elements, and the tower is simulated by beam elements. The wind turbine is replaced by a lumped mass element at the top of the tower, as shown in Figure 2.

Considering the effect of construction disturbance and long-term cyclic loading, a layer of frictional thin element is introduced into the soil surrounding the bucket [15–17]. The undrained strength of this layer of elements is αs_u, and reduction coefficient α is taken as 0.3. Frictional contact pairs are arranged between the bucket wall and the layer of thin element, which allows the interface to potentially break away and slip. The interface friction coefficient $\mu = 0.7$ is assumed. For the sake of comparison, the case with full interface adhesion, i.e., $\alpha = 1$, is also studied. In this case, the bucket wall and soil can not be permitted to separate and slip.

5. Displacement-Controlled Monotonic Loading

The ultimate capacity of bucket foundation under monotonic horizontal loading is analyzed. The finite element model is subjected to displacement-controlled pushover loading at the mass element; i.e., the height of application of the lateral displacement is $h = 80$ m. Two cases of $L/D = 0.2$

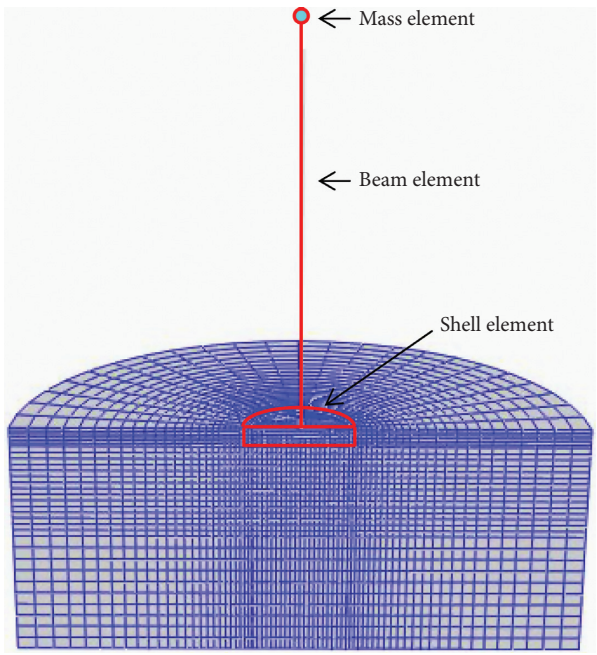

Figure 2: Finite element meshes.

and 0.6 are studied. The computed moment-rotation curves measured at ground level are shown in Figure 3. In Figure 3, $M = Fh$; $\theta = u/h$, where F and u are reaction force and lateral displacement at the action point. A is bottom area of the foundation, and s_{u0} is the undrained shear strength of soil at foundation base. In view of the strength profile selected in the paper, the value of s_{u0} is also 60 kPa for bucket foundation with aspect ratio $L/D = 0.6$ in nonuniform soil.

It is shown from Figure 3 that, considering the interface disturbance, the moment capacity is much lower than that when the interface is fully bonded. This shows that, in analyses of bucket foundation, the capacity obtained without considering the interface disturbance is too large, which leads to the unsafe foundation design. Through comparing Figure 3(a) with 3(b), it can be seen that the moment capacity increases with the increase of embedment. For example, when the aspect ratio increases from 0.2 to 0.6, the dimensionless moment capacity increases by about 80% for the fully bonded case. According to rough load estimates for an anticipated 3.5 MW wind turbine offshore the UK, the maximum overturning moment occurring at the seabed level is of the order of 120 MN [6]. It is noted that, for $L/D = 0.2$, the moment can be obtained as $M = 0.78ADs_{u0} = 294$ MN taking into account the imperfect interface. Therefore, The foundation design of low aspect ratio such as $L/D = 0.2$ meets the requirement in terms of bearing capacity.

By comparing Figure 3(b) with 3(c), the dimensionless capacity of foundation in heterogeneous soil is 13% and 26% lower than that in homogeneous soil for the case of full bonding and imperfect interface. The mechanism that the capacity is lower in heterogeneous soil relative to homogeneous soil is illustrated in Figure 4.

As shown in Figure 4, the instability mode of bucket foundation under lateral loads is generally in the form of rotation. In homogeneous soil, the arc-shaped slip surface is mainly located on the outside of the foundation and passes through the deep soil beneath the bucket. However, in the heterogeneous soil, the strength of shallow soil is relatively low; therefore the slip surface is limited to the shallow soil in the bucket, but not extended to the deep soil with higher strength.

6. Displacement-Controlled Cyclic Loading

To investigate the influence of interface conditions on the response of bucket foundation under cyclic loading, displacement-controlled cyclic loading is carried out for two aspect ratios of $L/D = 0.2$ and 0.6, respectively. Constant-amplitude displacement cycles are applied at the nacelle level of the 3.5 MW turbine, i.e., the mass element shown in Figure 2. The displacement cycle varies according to sinusoidal law with period $T = 10$ s. Two sets of analyses consisted of imposing displacement amplitudes that produced rotations of $\theta = 0.01$ rad and 0.05 rad, respectively. Figures 5 and 6 depict the cyclic moment-rotation graphs for both aspect ratios and interface conditions.

As shown in Figures 5 and 6, under small cyclic loading, the hysteresis loop formed by the moment-rotation relation curve is close to the elastic response, whereas the area of the hysteresis loop increases obviously under large cyclic loading. It is shown that there is a significant plastic deformation in the soil under large cyclic loading, which results in a larger energy dissipation in the soil-bucket coupling system, but the shape of the hysteresis loop is related to the interface condition. This conclusion is consistent with that of Kourkoulis et al. [5].

For the full bonding interface condition, the loading and unloading paths generally obey the Masing rule and follow the skeleton curve, i.e., the monotonic loading curve. However, under the imperfect interface condition, the loading and unloading paths after the first cycle deviate from the skeleton curve and tend to be flattened. The area surrounded by the hysteresis loop is lower than that produced under full bonding condition. This is attributed to the fact that, during the first cycle, there forms an unrecoverable gap between the loading side of the bucket and the surrounding soil, and then, under the subsequent cycles, the existence of these cracks leads to the reduction of the overall resistance.

7. Response to Environmental Loading

The bucket foundation for offshore wind turbines is subjected to long-term cyclic loading from wind and wave during the whole service period, and the soil around the foundation may produce strain accumulation or stiffness weakening, which will lead to excessive displacement of the foundation and affect the normal operation of the turbines. To ensure the normal operation of the fixed-bottom offshore wind turbines, the cumulative rotation angle of the foundation should not exceed 0.2°, i.e., approximately 3.5×10^{-3} rad [9]. So the main issue with bucket foundations under lateral cyclic loading is to predict how much rotation (or lateral displacement) will occur at given amplitude of

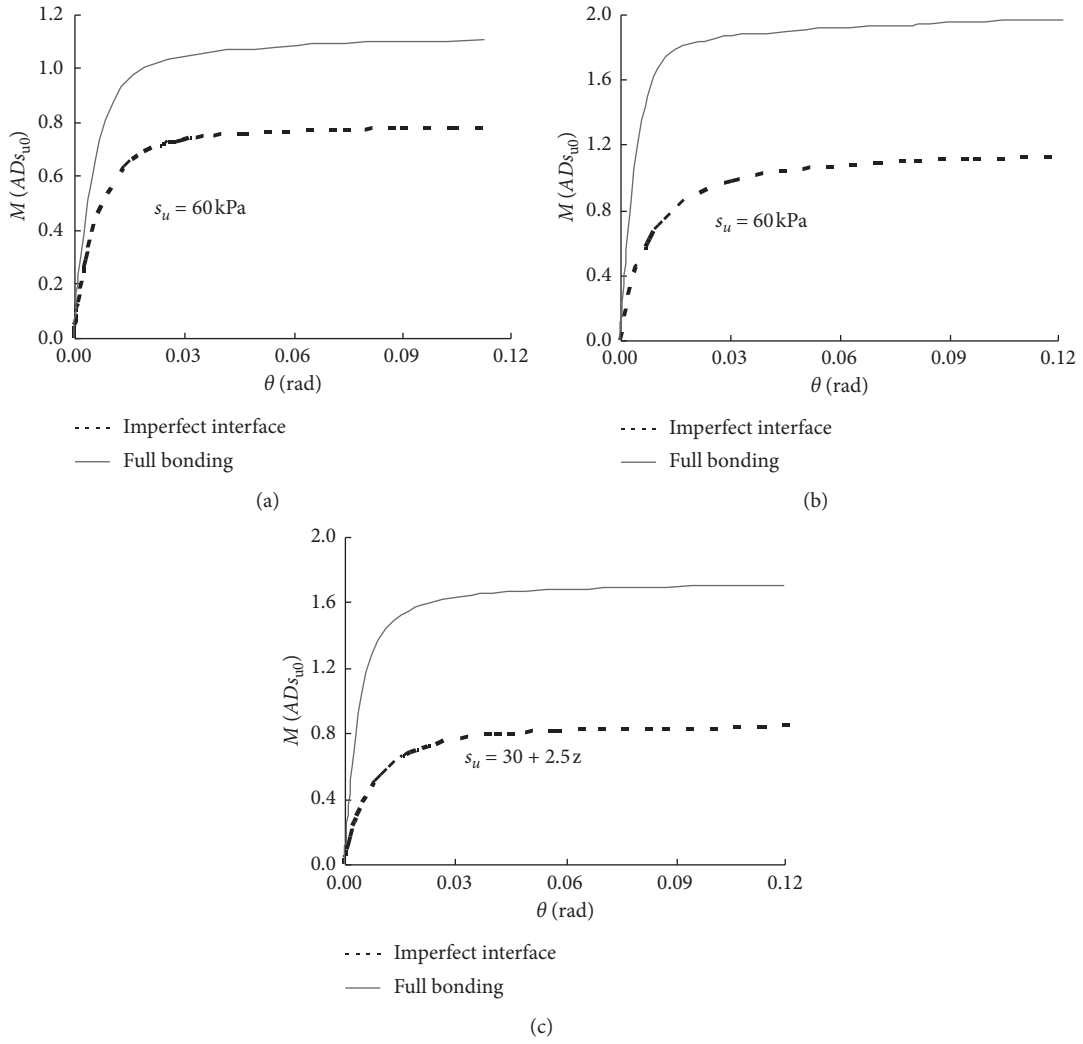

Figure 3: Relation of moment and rotation of bucket foundation subjected to monotonic loading. (a) $L/D = 0.2$. (b) $L/D = 0.6$ (homogeneous). (c) $L/D = 0.6$ (heterogeneous).

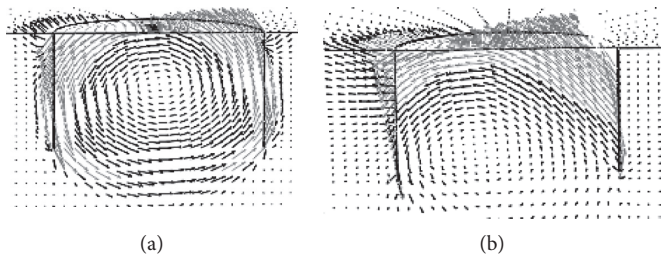

Figure 4: Failure mechanisms of bucket foundation. (a) Homogeneous. (b) Heterogeneous.

cyclic load. The wave loads have a period of the order of 10 seconds and can be simulated in a slow-cyclic manner. The wind load is generally acknowledged to be of much larger period; therefore it can be simulated in a quasistatic behavior.

In this section, for a typical 3.5 MW offshore wind turbine, it is assumed that the bucket foundation is founded at 15 m water depth. According to the current codes of practice, a design wind load of $F_{\text{wind}} = 1$ MN is assumed, acting on the center of the rotor-nacelle assembly, whose distance from mud-line is $h = 80$ m. The wind load is combined with a design wave load of $F_{\text{wave}} = 2 \sin \omega t$ (MN), acting on a height of $h = 7.8$ m from the mud-line. The circular frequency of wave load is $\omega = 2\pi/T$, in which T is wave period.

In the finite element analysis, the following loading scenario is adopted: monotonic loading due to wind, followed by one thousand cycles of loading due to waves.

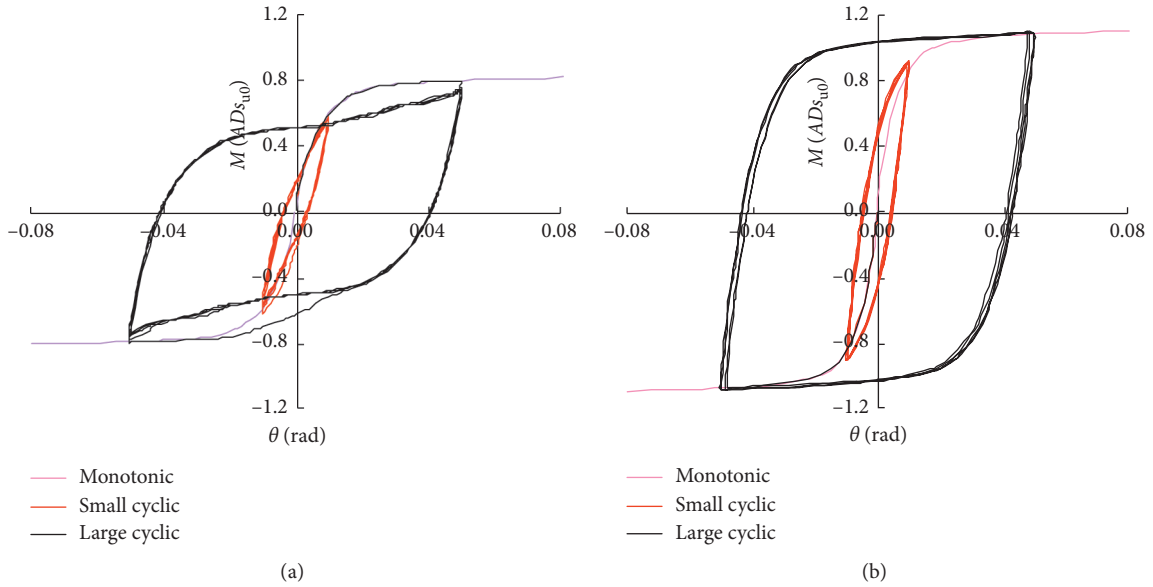

Figure 5: Relation of moment and rotation of bucket foundation of aspect ratio $L/D = 0.2$. (a) Imperfect interface. (b) Full bonding.

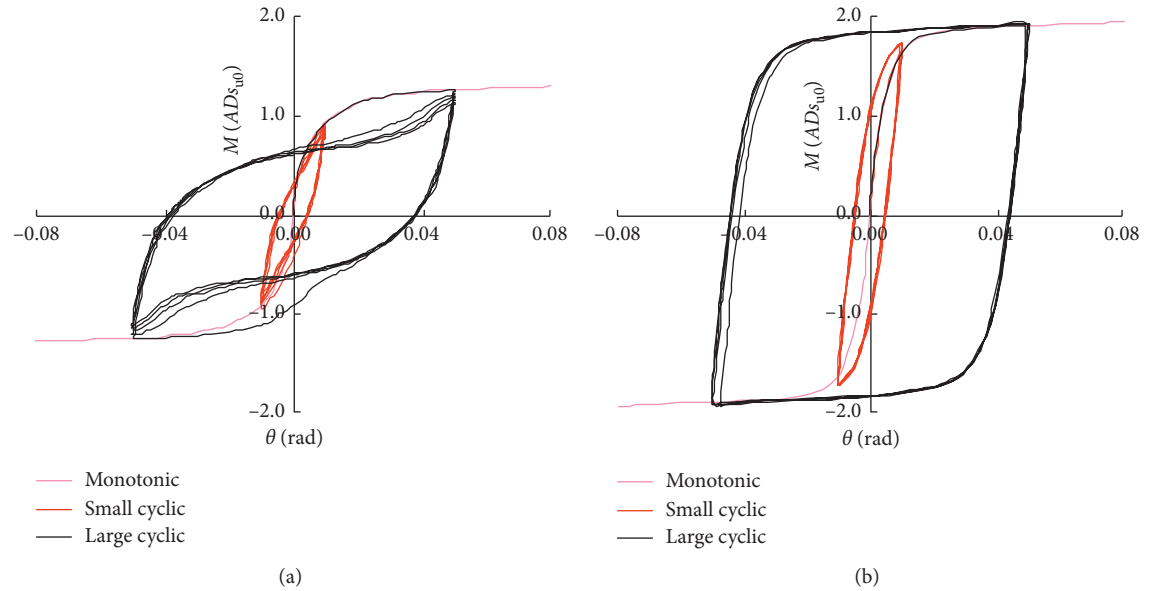

Figure 6: Relation of moment and rotation of bucket foundation of aspect ratio $L/D = 0.6$. (a) Imperfect interface. (b) Full bonding.

According to available results [18–20], the one-way cyclic loading has been generally shown to cause larger accumulation of plastic deformation than two-way cyclic loading, so the loading scenario adopted in this paper is more conservative. Thus, the rotation accumulation of bucket foundation with the number of cycles is obtained.

To keep the figure clear, the maximum, minimum, and average rotation angle during each cycle are given in Figures 7 and 8, corresponding to the top, bottom, and middle curve of each figure, respectively. The rotation angle of bucket foundation under cyclic loading is decomposed into residual component $\overline{\theta}$ and oscillatory component $\Delta\theta$:

$$\theta = \overline{\theta} + \Delta\theta. \tag{9}$$

It can be seen that, under thousands of loading cycles, the oscillatory component $\Delta\theta$ of the bucket foundation with low aspect ratio is smaller than the residual component $\overline{\theta}$, and the residual component $\overline{\theta}$ gradually accumulates until it exceeds the allowable value. The amount of oscillatory component $\Delta\theta$ is only 10% of the residual component $\overline{\theta}$. However, for bucket foundations of high aspect ratio, the ratio of oscillatory component to residual component increases to 23%~26%, but the accumulation rate of residual component decreases gradually before it tends to zero.

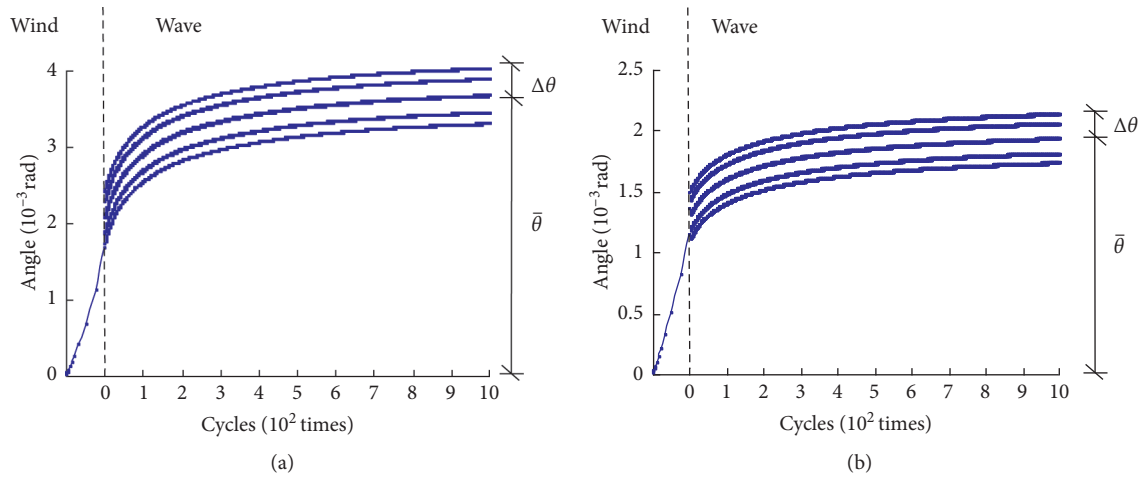

Figure 7: Relation of rotation and cyclic numbers of bucket foundation of aspect ratio $L/D = 0.2$. (a) Imperfect interface. (b) Full bonding.

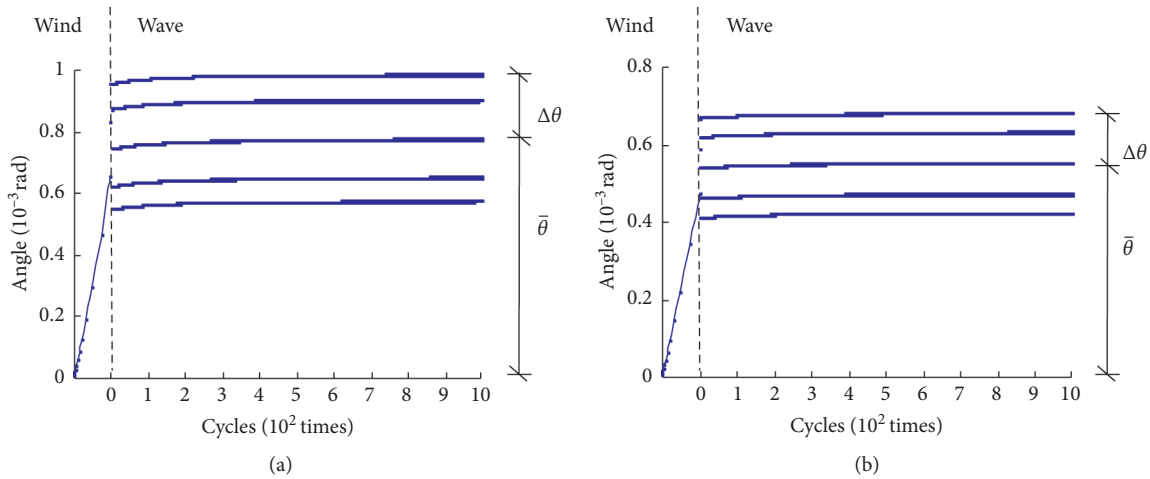

Figure 8: Relation of rotation and cyclic numbers of bucket foundation of aspect ratio $L/D = 0.6$. (a) Imperfect interface. (b) Full bonding.

From Figure 7(a), considering the case of imperfect interface, the accumulated rotation of bucket foundation with $L/D = 0.2$ subjected to one thousand cycles of lateral loading has exceeded the allowable rotation limit. In the case of full bonding, although the rotation under one thousand cycles of lateral loading does not reach the serviceability limit, the curve representing residual component shows a rising trend. Taking into account that an offshore wind turbine is expected to sustain approximately 10^8 cycles of loading over a period of 20 years of service [21–23], the rotation of bucket foundation with aspect ratio $L/D = 0.2$, in the case of full bonding, is still possible to exceed the allowable deformation limit. From Figure 8, it can be recognized that whether the interface is full bonding or not, the $L/D = 0.6$ footing maintains almost constant rotation despite the increasing number of cycles. The foundation with $L/D = 0.2$ and $D = 20$ m meets the requirement in terms of bearing capacity; however the accumulated rotation may exceed the allowable deformation limit during the service period; therefore it should be cautiously utilized in engineering practice.

8. Conclusion

The response of bucket foundations for offshore wind turbines subjected to cyclic loading in saturated clay is explored through three-dimensional finite element numerical analyses. The finite element model is validated against published in situ tests of bucket foundations under quasistatic cyclic loading in Bothkennar clay. The following conclusions can be drawn:

(1) Under displacement-controlled cyclic loading, for the cycles of low-amplitude rotation, dimensionless moment-rotation curve is approximately linear elastic; however the curve engenders significant hysteresis loop, whose shape is influenced by soil-sidewall interface condition, during high-amplitude cycles.

(2) Under thousands of loading cycles, for bucket foundations of low aspect ratio, the ratio of oscillatory displacement component to residual component is only 10%; however the residual component

will accumulate gradually until the serviceability rotation is exceeded. For foundations of high aspect ratio, the ratio of oscillatory component to residual component is relatively larger, but the accumulation rate of residual displacement decreases gradually.

(3) The bucket foundation of aspect ratio L/D lower than 0.2 meets the design requirement in terms of bearing capacity; however, the accumulated rotation may exceed the allowable deformation limit during the service period.

Data Availability

All the data in this paper are obtained from tests in this study, and no other data in the literature are used to support this study.

Conflicts of Interest

The authors declare no potential conflicts of interest with respect to the research, authorship, and/or publication of this article.

Acknowledgments

This research presented here was undertaken with support from Major Scientific and Technological Innovation Project of Key Research and Development Plan of Shandong Province (2019JZZY010125) and Shandong Natural Science Foundation Project (ZR2019MEE010, ZR2018BEE047, and ZR2017MEE007).

References

[1] K. Wu, M.-Y. Ma, M.-T. Luan et al., "Numerical analysis of bearing capacity behavior of bucket foundation subjected to torsion shear loading based on elasto-plastic FEM," *Journal of Basic Science and Engineering*, vol. 20, no. 5, pp. 777–786, 2012.

[2] M. Achmus, Y.-S. Kuo, and K. Abdel-Rahman, "Behavior of monopile foundations under cyclic lateral load," *Computers and Geotechnics*, vol. 36, no. 5, pp. 725–735, 2009.

[3] Q.-L. Fan, H.-T. Zhao, J. Zheng et al., "Stability of bucket foundations under non-coplanar combined loading," *Rock and Soil Mechanics*, vol. 34, no. 12, pp. 3643–3648, 2013.

[4] R. Liu, L. Wang, H.-Y. Ding et al., "Failure envelopes of large-diameter shallow buried bucket foundation in undrained saturated clay under combined loading conditions," *Chinese Journal of Geotechnical Engineering*, vol. 36, no. 1, pp. 146–154, 2014.

[5] R. S. Kourkoulis, P. C. Lekkakis, F. M. Gelagoti, and A. M. Kaynia, "Suction caisson foundations for offshore wind turbines subjected to wave and earthquake loading: effect of soil-foundation interface," *Géotechnique*, vol. 64, no. 3, pp. 171–185, 2014.

[6] G. T. Houlsby, R. B. Kelly, J. Huxtable, and B. W. Byrne, "Field trials of suction caissons in clay for offshore wind turbine foundations," *Géotechnique*, vol. 55, no. 4, pp. 287–296, 2005.

[7] R. B. Kelly, G. T. Houlsby, and B. W. Byrne, "Transient vertical loading of model suction caissons in a pressure chamber," *Géotechnique*, vol. 56, no. 10, pp. 665–675, 2006.

[8] B. Zhu, B. W. Byrne, and G. T. Houlsby, "Long-term lateral cyclic response of suction caisson foundations in sand," *Journal of Geotechnical and Geoenvironmental Engineering*, vol. 139, no. 1, pp. 73–83, 2013.

[9] S. Bhattacharya, D. Lombardi, and D. Muir Wood, "Similitude relationships for physical modelling of monopile-supported offshore wind turbines," *International Journal of Physical Modelling in Geotechnics*, vol. 11, no. 2, pp. 58–68, 2011.

[10] J. Lemaitre and J. L. Chaboche, *Mechanics of Solid Materials*, Cambridge University Press, Cambridge, UK, 1990.

[11] I. Anastasopoulos, F. Gelagoti, R. Kourkoulis, and G. Gazetas, "Simplified constitutive model for simulation of cyclic response of shallow foundations: validation against laboratory tests," *Journal of Geotechnical and Geoenvironmental Engineering*, vol. 137, no. 12, pp. 1154–1168, 2011.

[12] M.-S. Huang and Y. Liu, "Numerical analysis of axial cyclic degradation of a single pile in saturated soft soil based on nonlinear kinematic hardening constitutive model," *Chinese Journal of Geotechnical Engineering*, vol. 36, no. 12, pp. 2170–2178, 2014.

[13] S. Gajan, B. L. Kutter, J. D. Phalen, T. C. Hutchinson, and G. R. Martin, "Centrifuge modeling of load-deformation behavior of rocking shallow foundations," *Soil Dynamics and Earthquake Engineering*, vol. 25, no. 7–10, pp. 773–783, 2005.

[14] Q.-L. Fan and M.-T. Luan, "Failure envelopes of bucket foundation for offshore wind turbines in V-H-T loading space," *China Civil Engineering Journal*, vol. 43, no. 4, pp. 113–118, 2010.

[15] Q.-L. Fan and Y.-F. Gao, "Effect of reinforcement ratio and vertical load level on lateral capacity of bridge pile foundations," *Polish Maritime Research*, vol. 25, no. s3, pp. 120–126, 2018.

[16] M. Luan, X. Sun, X. Tang, Q. Fan, and K. T. Law, "Lateral bearing capacity of multi-bucket foundation in soft ground," *China Ocean Engineering*, vol. 24, no. 2, pp. 333–342, 2010.

[17] K. Wu, Q. Fan, D. Hao, R. Chen, and J. Liu, "Construction mechanics effect of submarine immersed tube tunnel subjected to different pore pressures based on numerical analysis," *Journal of the Balkan Tribological Association*, vol. 22, no. 3, pp. 2447–2453, 2016.

[18] K. Meng, C. Cui, and H. Li, "An ontology framework for pile integrity evaluation based on analytical methodology," *IEEE Access*, vol. 8, pp. 72158–2168, 2020.

[19] S.-S. Lin and J.-C. Liao, "Permanent strains of piles in sand due to cyclic lateral loads," *Journal of Geotechnical and Geoenvironmental Engineering*, vol. 125, no. 9, pp. 798–802, 1999.

[20] C. Leblanc, G. T. Houlsby, and B. W. Byrne, "Response of stiff piles in sand to long-term cyclic lateral loading," *Geotechnique*, vol. 60, no. 2, pp. 79–90, 2010.

[21] S. Nanda, I. Arthur, V. Sivakumar, and S. Donohue, "Monopiles subjected to uni- and multi-lateral cyclic loading," *Proceedings of the Institution of Civil Engineers-Geotechnical Engineering*, vol. 170, no. 3, pp. 246–258, 2018.

[22] I. Anastasopoulos and M. Theofilou, "On the development of a hybrid foundation for offshore wind turbines," in *Proceedings of the Frontiers in Offshore Geotechnics*, Taylor and Francis/Balkema, Amsterdam, The Netherlands, 2015.

[23] R. J. Jardine, "Geotechnics, energy and climate change: the 56th rankine lecture," *Géotechnique*, vol. 70, no. 1, pp. 3–59, 2020.